Langmuir

Article

pubs.acs.org/Langmuir

Generic Methods for Micrometer- And Nanometer-Scale Surface Derivatization Based on Photochemical Coupling of Primary Amines to Monolayers of Aryl Azides on Gold and Aluminum Oxide Surfaces

Osama El Zubir, Iain Barlow, Ehtsham Ul-Haq, Hairul A. Tajuddin,† Nicholas H. Williams,* and Graham J. Leggett*

Department of Chemistry, University of Sheffield, Brook Hill, Sheffield S3 7HF, U.K.

Supporting Information

ABSTRACT: A series of aryl azide terminated thiols and phosphonic acids has been synthesized, and used to prepare self-assembled monolayers on (respectively) gold and aluminum oxide surfaces. The rates of photoactivation were determined using contact angle measurement and X-ray photoelectron spectroscopy (XPS). The behavior of a diazirine functionalized aryl thiol was also studied. The rates of activation were found to be similar for all five adsorbates. However, the extent of photochemical coupling of a primary amine was significantly greater for the aryl azides than for the diazirine. A range of primary amines was successfully coupled to all of the azides with high yield. Little difference in reactivity was observed following perfluorination of the aromatic ring. Micrometer-scale patterns were fabricated by carrying out exposures of the aryl azide terminated SAMs through a mask submerged under a film of primary amine. Contrasting amines could be introduced to unreacted regions in a subsequent maskless step. A scanning near-field optical microscope was used to fabricate nanopatterns. Exposure of the azides to irradiation at 325 nm in air enabled selective deactivation of azides. The surrounding surface was functionalized with a primary amine in a maskless process; when a protein-resistant oligo(ethylene glycol) functionalized amine was used it was possible to produce protein nanopatterns, by adsorbing protein to features defined using near-field exposure.

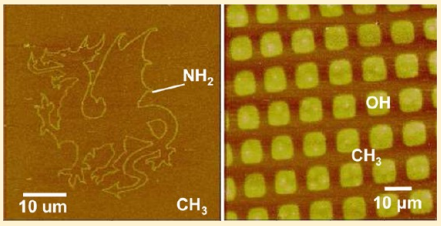

INTRODUCTION

The top-down modification of inorganic materials using techniques such as electron beam lithography and photolithography is well-established. However, for molecular materials, such methods have limited utility. For example, the stripping of resist requires the use of organic solvents that may be incompatible with biomolecules and with many organic film chemistries. Moreover, in many areas of molecular nanoscience, there is an urgent need for techniques that facilitate the direct manipulation of chemical structure and reactivity with a spatial resolution of a few tens of nm. Conventional lithographic techniques enable precise physical placement of functional elements but provide only limited means to control surface reactivity. This has led to the search for alternative approaches to nanolithography that are compatible with organic and biological molecules. Dip-pen nanolithography[1−3] and nanografting[4,5] facilitate precise placement and removal of molecular adsorbates. However, for the local, direct initiation of chemical reactivity, approaches based on the use of electrochemical reactions (for example, the local oxidation of adsorbates[6,7] or the potential-controlled deprotection of a surface[8]) and photochemistry (for example, using near-field optical techniques)[9−13] offer significant potential.

Photochemistry is a long-established tool in synthetic chemistry. Many functional groups undergo light-induced reactions, and a wide range of photocleavable protecting groups is available. The development of light-directed chemical synthesis[14] has provided a paradigm for the integration of top-down and bottom-up fabrication methods at the micrometer scale, and there is now a burgeoning literature describing a wide range of strategies for the photochemical control of reactivity at micrometer-length scales. Nitrobenzyl protecting groups have attracted a significant amount of interest,[15,16] enabling the selective uncaging of reactive functional groups such as amines[13,17,18] carboxylates,[19−21] and biologically functional groups such as biotin,[22,23] peptides,[24] and chelators of histidine residues.[25] However, other approaches, such as the use of thiol−ene chemistry[26] and photoactivated cycloaddition reactions[27] are also attracting attention.

Azides have recently attracted interest for 1,3-dipolar cycloadditions,[28] the most important of the so-called "click" reactions.[29] However, azides are also useful photoactive organic functional groups that are converted to nitrenes by exposure to UV light (or heat).[30,31] Azide precursors for nitrenes such as azidobenzal cyclohexanone ("ABC") are also used as efficient photo-cross-linkers for photoresist polymers.[32] In principle, the nitrene should be reactive toward a wide range of targets and the photochemical reactions of aryl azides in solution have been comprehensively studied. In practice, phenyl azide is regarded as a comparatively poor reagent for photoaffinity studies

Received: September 18, 2012
Revised: November 20, 2012
Published: December 17, 2012

   dx.doi.org/10.1021/la303746e | *Langmuir* 2013, 29, 1083−1092

because it tends to undergo rearrangement to form ketenimine rapidly at ambient temperature. The first step in the photoreaction (see Scheme 1) is the elimination of molecular

Scheme 1. Photochemistry of Aryl Azides

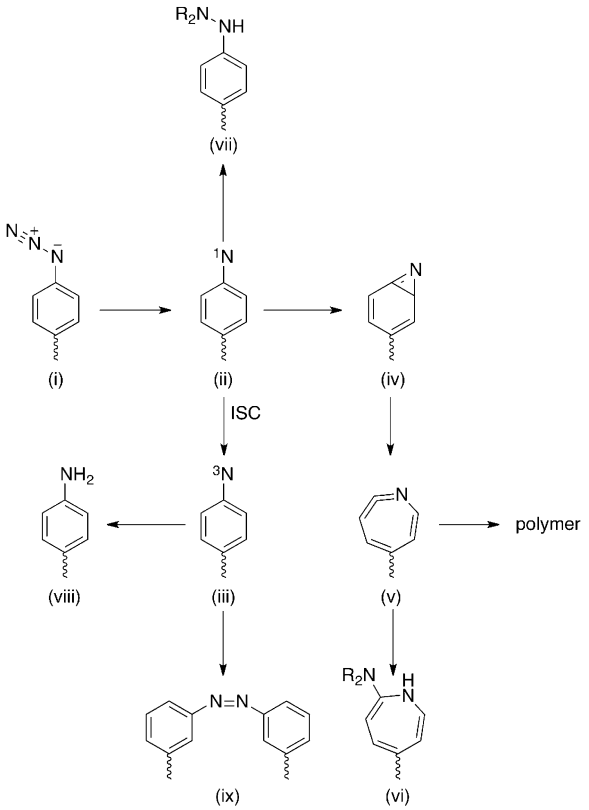

nitrogen from phenyl azide (**i**) to yield a singlet nitrene (**ii**). The singlet nitrene either undergoes intersystem crossing to a triplet (**iii**) phenyl nitrene or rearranges to form benzazirine (iv), which in turn rearranges to yield ketenimine (**v**). The ketenimine reacts readily with secondary amines to produce 2-amino-3H-azepines (**vi**),[33] with itself or (**i**) to form polymers, or it can revert back to the singlet nitrene (**ii**) and eventually irreversibly form the more stable triplet (**iii**). Singlet phenyl nitrene may form phenyl hydrazine (**vii**) in the presence of amines, according to some reports.[34,35] 2-Dehydroazepine may also be produced via a photochemical reaction of the triplet phenyl nitrene (**iii**),[36] which may also react to give anilines (**viii**) and diaryl diazo compounds (**ix**).[34−38] Intersystem crossing (ISC), which converts the singlet phenyl nitrene to the triplet nitrene dominates at 77 K, whereas the singlet phenyl nitrene favors ring expansion to (**iv**) at room temperature. Therefore, the ring expansion of an aryl singlet nitrene is dependent on the reaction temperature.[36,39,40] The preferred product distribution of any particular aryl azide is markedly influenced by the substituents that are present on the aromatic ring and the conditions of the experiment [for example, strongly electron donating substituents and hydroxylic solvents enhance ISC from (**ii**) to (**iii**)]. Finally, under acidic conditions, the singlet nitrene can capture a proton to generate an electrophilic nitrenium ion.[41,42] In terms of trapping reactions, the dominant pathways to covalently capture organic compounds stem from the singlet state, with ISC to the triplet providing a relatively slow competing pathway. These reactions usually involve insertion reactions or addition reactions with nucleophiles. In the absence of external reagents, the nitrene decomposes through a variety of pathways to a number of stable species.[43,44]

There are some reports of the use of aryl azide functionalized surfaces for surface immobilization. For example, Wrighton and co-workers immobilized redox-active functional groups onto SAMs, and there has been some interest in the use of aryl azides for the immobilization of biological molecules onto solid supports.[45,46] More recently, Yan and co-workers have reported a variety of bioconjugation strategies based around perfluoroazides. They have demonstrated the coupling of furanones[47] and carbohydrates[48,49] to surfaces functionalized with perfluoroaryl azides, via a nonspecific reaction. Cross-linking to carbon−carbon double bonds and polymers that lack reactive functional groups has also been demonstrated.[50] One motivation for the use of a perfluoaryl azide is the previously reported stabilization of the singlet excited state by ring halogen substituents, tending to suppress the ring expansion reaction shown above and causing an enhanced rate of reaction between the nitrene species and molecules in solution, instead.

The present work is focused on the attachment of primary, not secondary, amines to surfaces. We have discovered that the capture of UV photons is extremely efficient, enabling rapid, selective reactions to be carried out with a wide range of primary amines, providing a simple general method for the introduction of new functional groups to surfaces that is easily combined with surface patterning. The wide variety of primary amines that are readily available and compatible with a variety of solvents means that such strategies have promise for micro- and nanofabrication. We have investigated the effect of ring substitution on these reactions and also compared this behavior with a diazirine-functionalized monolayer, which yields a carbene upon UV excitation, expected to exhibit similar generalized reactivity to an azide. Micrometer-scale photopatterning and nanometer-scale patterning using near-field optical techniques have been investigated.

EXPERIMENTAL SECTION

All chemicals were purchased from Sigma-Aldrich, Alfa Aesar, and Fisher Scientific, unless otherwise stated and used as received. NeutrAvidin conjugated yellow-green fluorescent (505/515) nanoparticles (1% solids) were obtained from Invitrogen Molecular Probes (Paisley, U.K.). Immersol 518 F fluorescence-free immersion oil and Citifluor glycerol/PBS solution mounting media were purchased from Carl Zeiss and Citifluor Ltd., respectively. Common solvents were dried using a Grubb's solvent purification system. Detailed synthetic protocols and characterization data are given in the Supporting Information.

Gold wire (99.99%) was purchased from Goodfellow Metals (Cambridge, U.K.). All evaporation boats (molybdenum boats for currents of 35 A for gold deposition, and tungsten at currents of 55 A for aluminum), chromium chips (99.99%), and SEM grids (ranging from 400 to 2000 mesh, Cu gauze; Maxtaform HF15, Cu: Rh gauze) were purchased from Agar Scientific (Cambridge, U.K.). Ultrahigh purity (UHP) water was obtained using a two-stage purification system using an Elga Purelab Ultra Bioscience polisher (Veolia Water) giving a final water resistance of 18.2 MΩ.

Metal films were thermally evaporated using an Auto 306 evaporator (BOC-Edwards, Crawley, U.K.), held at a maximum pressure of 1×10^{-6} mbar prior to metal evaporation. SAMs were prepared by immersing an Au-coated, Cr-primed glass coverslip (Chance-Proper no. 2) into a 1.0 mM ethanol solution of the appropriate thiol overnight. Glass coverslips were cleaned prior to evaporation in piranha solution (7:3 H_2SO_4:100 vol H_2O_2, caution:

dx.doi.org/10.1021/la303746e | Langmuir 2013, 29, 1083−1092

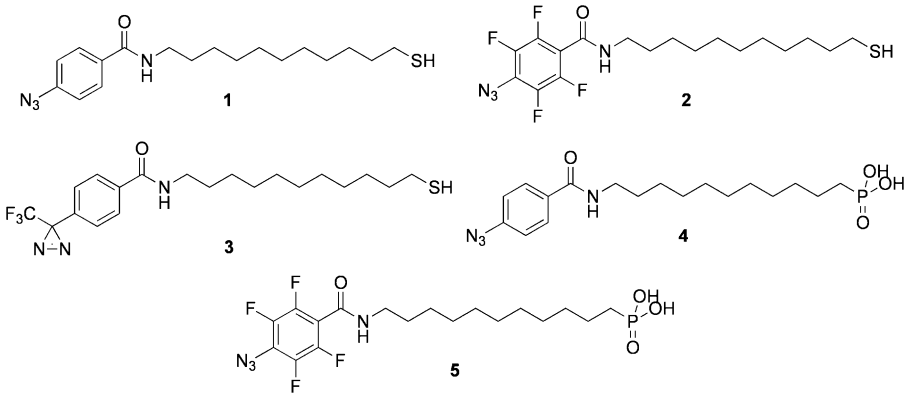

Figure 1. Adsorbates used in the present study.

explosive upon contact with organic materials), rinsed copiously with UHP water, and dried in a 120 °C oven overnight.

SAMs of phosphonic acids on Al_2O_3 were prepared by evaporation of Al onto a clean Cr-primed glass coverslip. The Al slide was allowed to anneal in air for 1 h to build an oxide layer, before being immersed in a 1.0 mM ethanol solution of the appropriate phosphonic acid overnight.

Contact angle goniometry was performed on a NRL CA goniometer (100-00-230, Ramé-Hart, Mountain Lakes, NJ), using the sessile drop method with UHP water. Contact angles are reported as mean values of 10 measurements.

X-ray photoelectron spectroscopy (XPS) analysis was carried out on a Kratos Axis Ultra instrument (Kratos, Manchester, U.K.), operating at a base pressure of 1×10^{-9} mbar. Survey spectra were acquired at a pass energy of 160 eV, and high resolution spectra of the individual core orbitals were acquired at a pass energy of 20 eV. All XPS spectra were analyzed and curve-fitted using Casa XPS[51] and were corrected relative to the C 1s signal at binding energy (B.E.) = 285.0 eV.

Friction force microscopy (FFM) images were acquired on a Nanoscope III Multimode atomic force microscope (Veeco, Cambridge, U.K.), using unfunctionalized Si_3N_4 cantilevers (NP-10, nominal spring constant 0.06 N m^{-1}, Veeco).

Samples were irradiated using an He−Cd laser, (IK 3202R-D, Kimmon, Tokyo, Japan), operating at λ = 325 nm. For scanning near-field photolithography, the laser was coupled to an AlphaSNOM scanning near-field optical microscope stage (Witec, Ulm, Germany).

RESULTS AND DISCUSSION

Synthesis of Thiols. The design of adsorbates for the capture of solution-borne amines required the incorporation of the photoaffinity labeling functionality as the tail group of the adsorbate to maximize the exposure of the reactive intermediate to the trapping solution. Along with the thiol and phosphonic acid moieties for anchoring to gold and aluminum oxide, respectively, the link to the chromophore must be stable under the immobilization conditions. Therefore, thiols **1**−**3** (Figure 1) and phosphonic acids **4** and **5** were identified for study. The synthesis of these compounds is described in detail in the Supporting Information.

In addition to aryl azide **1**, tetrafluoro analogue **2** was synthesized, as tetrafluoro substitution reduces the rate of the competing ring expansion pathway that occurs very rapidly in unsubstituted aryl azides.[52−55] Diazirine **3**, which undergoes the loss of N_2 on irradiation to generate a more reactive carbene, was studied to determine if this property affected the trapping efficiency.

Irradiation of Monolayers Under Ambient Conditions. To estimate the rate of photomodification of the monolayers and identify suitable exposures for carrying out surface coupling reactions, samples were irradiated by light from an HeCd laser (325 nm) under ambient conditions, and the changes in the advancing water contact angle were measured. Figure 2 shows data for azide and diazirine functionalized SAMs adsorbed on gold surfaces.

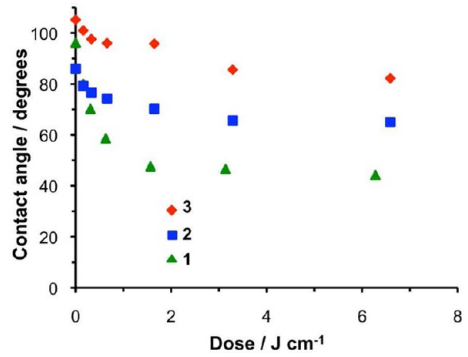

Figure 2. Variation in the water contact angle with an irradiation dose at 325 nm for photosensitive SAMs on gold. Red diamonds indicate data for the diazirine terminated thiol, and the green triangles and blue squares represent data for the azide and the perfluorinated azide, respectively. The errors are smaller than the symbols used to mark data points.

As-prepared films of the phenylazide, perfluorophenylazide, and diazirine (**1**−**3**) on gold yielded water contact angles of 96, 86, and 105°, respectively (Figure 2). As expected, the diazirine monolayer, which presented a CF_3 group at its surface, has the largest contact angle. After exposure to UV light, the contact angle for **1** was observed to decrease, approaching a limiting value of ca. 44° after an exposure between 3 and 6 J cm^{-2}. The perfluoro azide **2** yielded a slightly higher limiting contact angle (65°) than **1**, after a very similar exposure. The diaziridine **3** yielded a limiting contact angle that was somewhat larger, ca. 82°. However, the rate of photomodification was very similar to that of **1** and **2**, suggesting that the rate of modification was in all cases strongly influenced by the cross section for absorption of a UV photon by the aromatic ring. The kinetics were modeled a variety of ways, using both cos θ (proportional to the surface free energy) and the XPS peak areas as a measure of the extent of photomodification. However, a good fit to the data could not be obtained with any simple model, suggesting that the extent of photomodification does not depend in a simple way on the exposure (perhaps because of the wide

dx.doi.org/10.1021/la303746e | Langmuir 2013, 29, 1083−1092

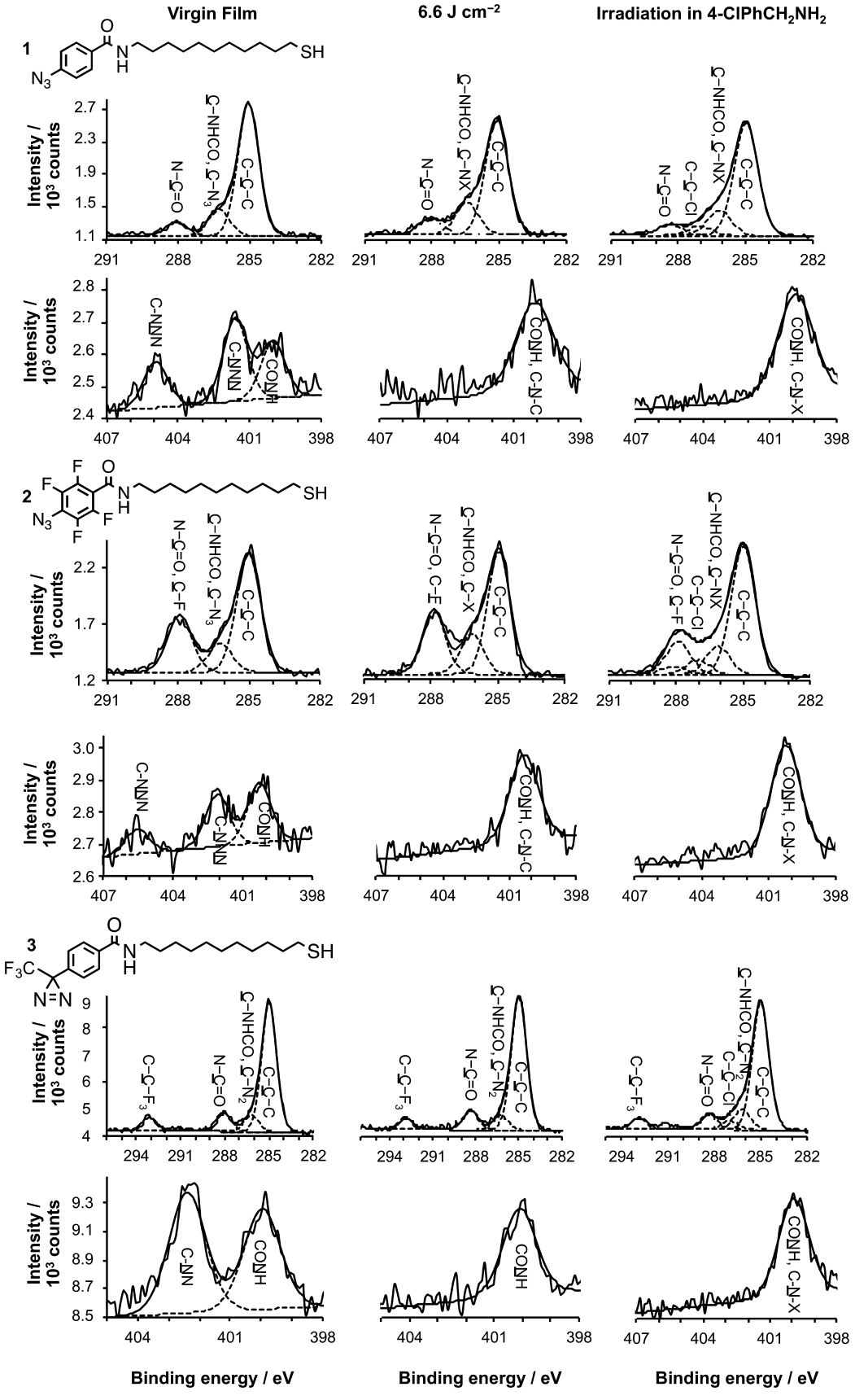

Figure 3. XPS C 1s and N 1s spectra for monolayers of aryl azide and diazirine functionalized alkylthiolates adsorbed on gold surfaces before (left-hand column) and after (center) exposure to UV light and after (right) exposure to UV light under a solution of 4-chlorobenzylamine.

dx.doi.org/10.1021/la303746e | *Langmuir* 2013, 29, 1083−1092

variety of excitation pathways that are accessible, as shown in Scheme 1).

X-ray photoelectron spectra were recorded for SAMs on Au before and after exposure to UV light. C 1s spectra (Figure 3) exhibited the expected features. All three compounds, **1** − **3**, showed strong peaks at 285 eV, corresponding to the carbon atoms in the aromatic ring and in the alkyl linker to the headgroup and a peak at ca. 288 eV, corresponding to the amide carbon atom. In the case of the perfluorinated aryl azide **2**, a substantial overlapping contribution was observed that was attributed to the ring carbons bonded to fluorine, and a corresponding small reduction was observed in the size of the peak at 285 eV. Between the main carbon peak and the amide carbon peak, a peak was observed at ca. 286.5 eV that was attributed to the carbon atoms adjacent to the azide and adjacent to the amide nitrogen. Finally, the diazirine exhibited a peak at ca. 293 eV that was attributed to the carbon atom in the terminal CF_3 group. No significant changes were observed in the C 1s spectra following exposure to UV radiation.

However, substantial changes were observed in the N 1s region following UV exposure (Figure 4). Virgin films of both

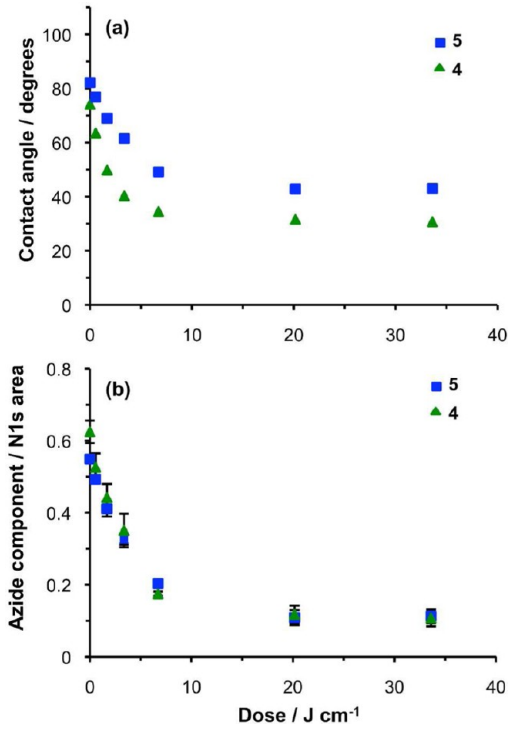

Figure 4. (a) Variation in the water contact angle with an irradiation dose at 325 nm for photosensitive SAMs on aluminum oxide. (b) Variation in the size of the azide component in the N 1s spectrum, as a fraction of the total N 1s peak area, as a function of exposure. The green triangles and blue squares represent data for the azide and the perfluorinated azide, respectively. The errors in (a) are smaller than the symbols used to mark data points.

aryl azides yielded spectra that were fitted with three components at 399, 402, and 405 eV in the ratios 1:2:1, respectively. The peak at the smallest binding energy was attributed to the amide nitrogen atom, while the peak at the highest binding energy was attributed to the central nitrogen atom in the azide group, which carries a partial positive charge. The other two nitrogen atoms yielded overlapping peaks at ca. 402 eV. After exposure to UV light, the area of the N 1s peak was reduced by approximately 50%, consistent with the elimination of N_2, and a single peak was observed centered on ca. 400 eV, attributed to the combined intensities of the nitrogen atoms in the amide group and the photomodified nitrene. The product of the degradation process could be amines formed by reduction of the photochemically generated nitrene, diazo compounds formed by dimerization of neighboring nitrenes, or more complex polymers formed by the reactions of nitrenes with neighboring azides (or through ketenamine reactions with themselves in the absence of good nucleophiles).[43]

Monolayers of aryl azide-terminated phosphonates on aluminum oxide yielded slightly smaller contact angles than SAMs of aryl azide-terminated thiols on gold, possibly indicating that they were more closely packed. In general, monolayers of *n*-alkylphosphonates are thought to pack more closely on aluminum oxide surfaces than do monolayers of alkylthiolates with similar chain lengths. In the present case, closer packing of the adsorbates would be expected to lead to the polar azide terminal group exerting a greater influence on the surface properties, and this would be expected to increase the interfacial free energy. However, the adsorbates with perfluorinated aryl rings still yielded larger contact angles on aluminum oxide surfaces, suggesting that the character of the ring still contributes to the interfacial tension. It is possible that the aromatic ring is canted,[56] as has been reported on alkylthiolate surfaces.

Figure 4a shows the variation in the advancing water contact angles of aryl azide terminated alkylphosphonate SAMs on aluminum oxide, following UV exposure. The contact angles fell rapidly at first, approaching a limiting value after an exposure of ca. 6 J cm^{-2}, similar to the dose required for the analogous adsorbates on gold (the variation in cos θ with exposure is shown for films on both Au and Al in the Supporting Information), indicating that the photochemistry is dominated by the nature of the terminal group of the adsorbate molecule, rather than the substrate−adsorbate interaction.

Similar changes were observed in the N 1s spectra to those described above for SAMs of aryl azide-terminated thiols, with the peaks at 402 and 405 eV disappearing and the peak at 399 eV increasing in size due to the formation of the photodegradation products (whether amines or polymers). The degree of modification could be quantified straightforwardly by measuring the ratio of the azide component in the N 1s spectrum to the total N 1s peak area. Figure 4b shows data for SAMs of **4** and **5**. The size of the azide component in the N 1s spectrum decreased with exposure, approaching a limiting value after a dose of ca. 6 J cm^{-2}, consistent with the changes in contact angle.

Photochemical Surface Immobilization of Amines. The reactivity of the photosensitive adsorbates toward primary amines was investigated. Samples were placed in a quartz cell, sealed with a Viton O-ring, immersed under a film of 4-chlorobenzylamine, and exposed to 6.6 J cm^{-2} UV light. X-ray photoelectron spectra were acquired. Figure 5 shows the Cl 2p region of the XPS spectrum for virgin and modified samples. For all of **1**, **2**, and **3**, a Cl 2p peak is plainly observed after completion of the reaction, indicating incorporation of 4-chlorobenzylamine at the surface. In the C 1s region, a new component was observed at ca. 287 eV, corresponding to the carbon atom adjacent to chlorine in 4-chlorobenzylamine. For the diazirine-functionalized surface, a peak was still evident at 293 eV that was attributed to the carbon atom in the CF_3

dx.doi.org/10.1021/la303746e | *Langmuir* 2013, 29, 1083−1092

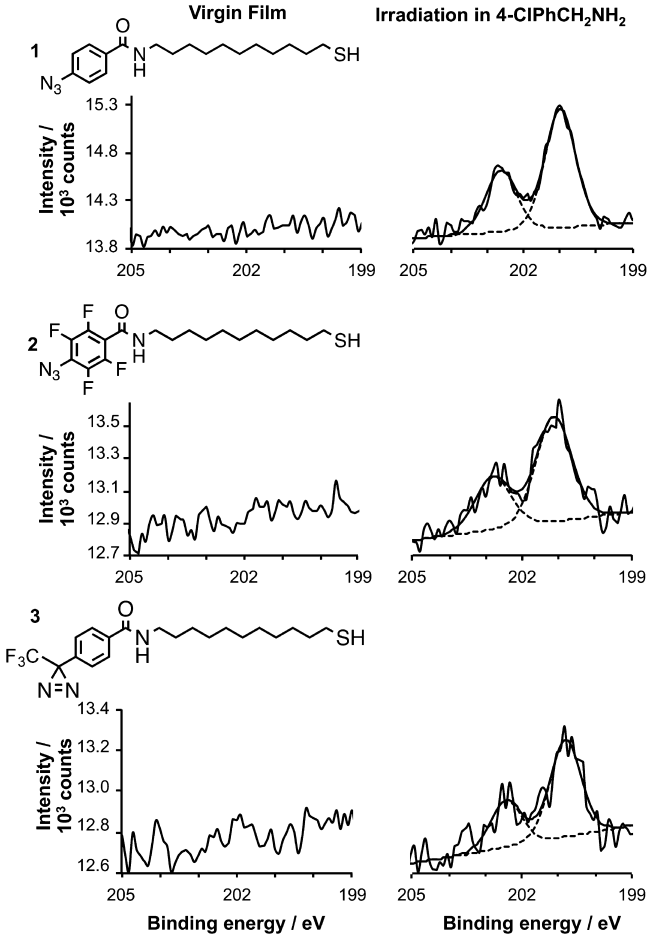

Figure 5. Cl 2p spectra for SAMs of **1**−**3** following exposure to UV light under 4-chlorobenzylamine.

group, and the C−C−Cl was somewhat smaller than this peak, indicating a limited degree of derivatization. However, for both of the aryl azides, the C−C−Cl component in the spectrum was somewhat larger. For **1**, it was close in size to the peak from the carbon in the amide group; for **2** it was slightly smaller in size but still substantial. Quantitative data are tabulated in the Supporting Information. The ratio of the intensity of the carbon adjacent to the chlorine atom to the area of the main hydrocarbon peak in the C 1s spectrum would be 1:14 for a coupling efficiency of 100%. A ratio of 1:19 was measured for **1** (74% of the calculated value) and a value of 1:13 was obtained for **2** (indicating close to 100% derivatization). However, there will have been some attenuation of the photoelectrons from the alkyl chain, meaning that the relative contribution of the C−C−Cl component to the spectrum will be slightly increased, and in both cases the degree of derivatization is probably slightly less than the calculated value. For the diazirine, a ratio of 1:16 would be expected for 100% reaction with 4-chlorobenzylamine; a ratio of 1:27 was measured, suggesting ca. 50% reaction (allowing for a small amount of attenuation of the signal from the lower lying carbon atoms in the adsorbate layer). This still represents a high degree of surface functionalization, albeit less than is observed for the aryl azides.

The reactivity of aryl azide-terminated SAMs on aluminum oxide surfaces to primary amines was also confirmed by XPS. Figure 6 shows the C 1s, N 1s, and F 1s regions of the spectra of samples 11-[(4-azido-benzoylamino)-undecyl]-phosphonate **4** before (top row) and after (bottom row) exposure to UV light while the sample was immersed in 2,2,2-trifluoroethylamine. The appearance of a peak in the C 1s region of the spectrum at ca. 292.7 eV (that could not be displaced by washing) and the appearance of a strong F 1s peak indicates that the amine has become coupled to the surface. Consistent with this, the N 1s region shows a loss of the peaks at 401.1 and 404.5 eV, corresponding to the azide following UV exposure,

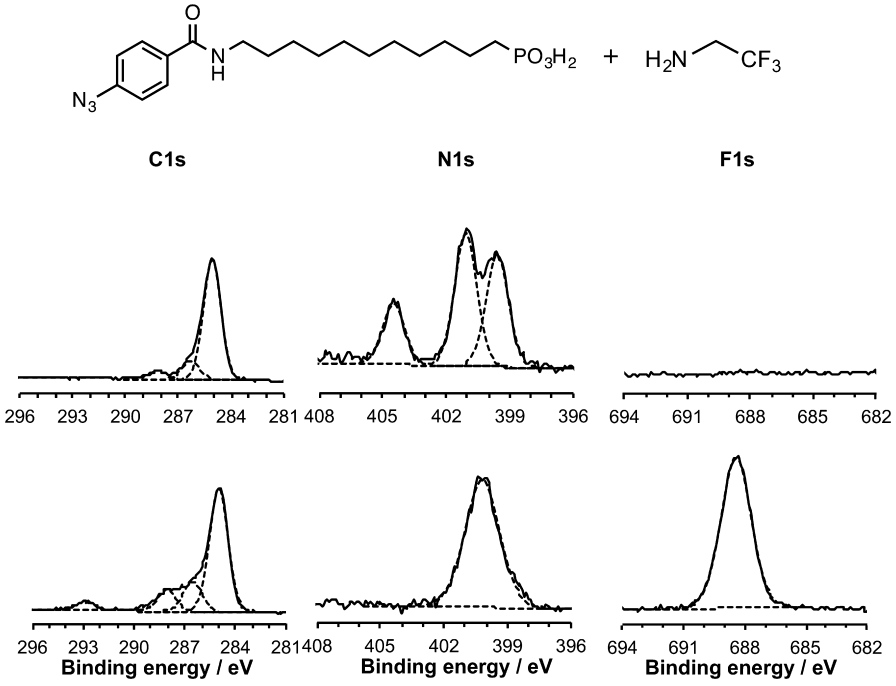

Figure 6. XPS spectra for SAMs of 11-[(4-azido-benzoylamino)-undecyl]-phosphonate on aluminum oxide **4** before (top) and after (bottom) exposure to UV light under 2,2,2-trifluorethylamine.

dx.doi.org/10.1021/la303746e | *Langmuir* 2013, 29, 1083−1092

and the spectrum of the modified film exhibits a single peak at 399.6 eV.

To further examine the general utility of azide photocoupling reactions for surface functionalization, SAMs of adsorbates with aryl azide terminal groups were exposed to UV light under a variety of liquid amines. Contact angles were measured and are shown in Figure 7. Data are shown for aryl azides on aluminum

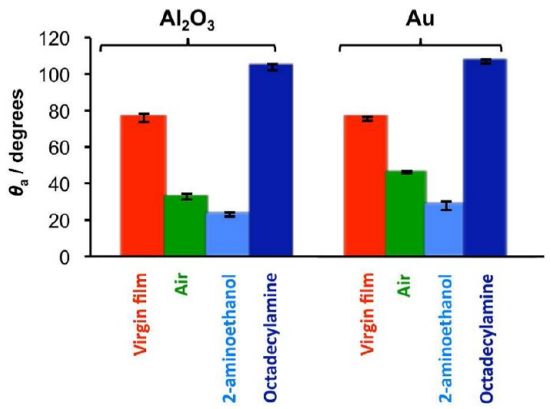

Figure 7. Contact angles of aryl azide SAMs formed by the adsorption of **1** and **4** following exposure to UV light in air, under ethanolamine and under octadecylamine.

oxide and on gold. Exposure under ethanolamine yielded a very small contact angle (23° on aluminum oxide and 28° on gold). This is consistent with coupling to the surface, predominantly via the amine, because the contact angles of amine-terminated surfaces are typically larger than this. As a control, the contact angle was measured for films of aminopropyltriethoxysilane on glass and found to be ca. 44°. In contrast, alcohol-terminated surfaces generally yield smaller contact angles. Hydrophobic surfaces could be created by exposing the SAMs to UV light under a solution of octadecylamine in chloroform. Contact angles of 104° and 108° were measured after exposure of SAMs on aluminum oxide and gold, respectively. Although these values are slightly smaller than, for example, the contact angle of a complete SAM of octadecanethiol on gold (ca. 115°), perfect films are not expected to result from a kinetic process and contact angles this large probably indicate extensive reaction between the amine and the surface azide. The nature of the trapping reaction could be through an insertion reaction that is preferential for the NH bonds, or could be through the formation of the electrophilic ketenimine that reacts with the more nucleophilic primary amine. The small difference in coupling efficiency between **1** and its fluorinated analogue **2** is not decisive in assigning either pathway. However, the expected shorter persistence of the singlet state generated from **1** does not appear to significantly decrease the fraction of surface, suggesting that inhibiting the ring expansion process is not particularly damaging to the immobilization of amines from solution. Although **2** forms the ketenimine more slowly than **1**, it is more reactive, and so overall slower conversion followed by very effective trapping may lead to a similar derivatization level to **1**. Thus, the immobilization of the primary amines that we have examined might be related to the nucleophilic properties of this functional group, allowing selective functionalization through this point in the molecule. The contrast with the more reactive carbene would be consistent with this analysis, although it is possible that intramonolayer reactions compete more effectively with trapping of solution components when the intermediate is more reactive, leading to lower derivatization.

Patterning. Micrometer-scale patterns were formed by exposing aryl azide terminated SAMs to UV light through a mask (an electron microscope grid), while submerged under a film of a primary amine. The amine and the mask were then removed, and the sample was rinsed and placed under a film of a second, contrasting amine. The sample was exposed to UV light in this second, maskless step. The process is shown schematically in Figure 8. The first step was designed to yield functionalization of the surface in a spatially selective fashion (i.e., in the regions exposed to UV light through the mask). The second step was intended to derivatize any remaining reactive sites with the contrasting amine.

The samples were imaged subsequently using friction force microscopy (FFM).[57−59] FFM yields differential contrast that can be related to variations in the surface free energy:[60] regions with high surface free energy exhibit bright contrast in friction images, and regions with low surface free energy exhibit dark contrast. In Figure 8 (panels a and c), bright contrast is observed in regions exposed to UV light while under a film of ethanolamine (squares), and dark contrast is observed in the

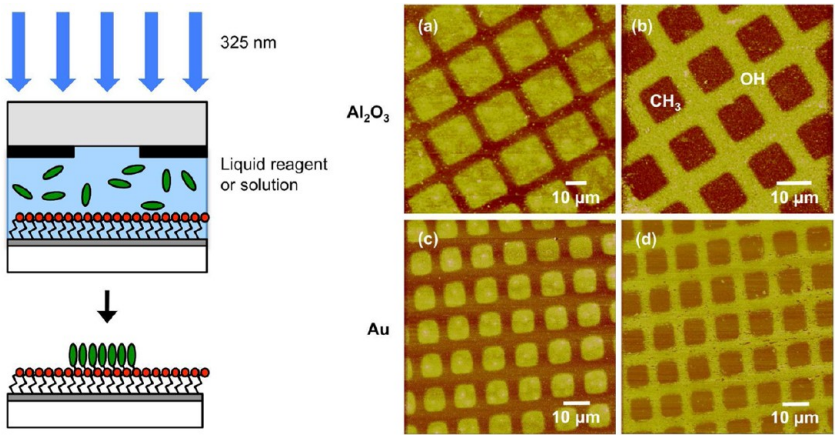

Figure 8. Schematic diagram showing the process used to fabricate two-component micrometer-scale patterns and (a−d) friction force microscopy images of aryl azide-terminated SAMs on (a and b) aluminum oxide and (c and d) gold following initial mask-based exposure under (a and c) ethanolamine or (b and d) octadecylamine followed by maskless exposure under either (a and c) octadecylamine or (b and d) ethanolamine.

dx.doi.org/10.1021/la303746e | *Langmuir* 2013, 29, 1083−1092

bars, which were masked from the UV irradiation during the first exposure but exposed during the second step while the sample was immersed under octadecylamine. Coupling of octadecylamine to the surface yields a low surface free energy and, hence, dark contrast in the friction image. Reversing the process yields an image with inverted contrast, indicating that octadecylamine has been coupled to the square regions (dark contrast, low friction), and ethanolamine has been coupled to the bars (Figure 8, panels b and d). The contrast difference between the regions derivatized with ethanolamine and octadecylamine is slightly greater on aluminum oxide than on gold, probably because of the slightly closer packing of the adsorbates.

Nanopatterning was carried out using a scanning near-field optical microscope (SNOM) coupled to the HeCd laser. It was hypothesized that the sample would interact with the near-field associated with the subwavelength aperture at the apex of the near-field probe, enabling high-resolution photolithography to be conducted as has been reported for films of alkylthiolates[9−11] and siloxanes.[13,18] Because near fields are not diffracted, the resolution of the lithographic process should not be limited by diffraction effects but, to a first approximation, by the diameter of the aperture in the probe.[12] The instrument employed in this work utilized a commercial cantilevered probe, with a pyramidal tip. The tip was coated with Al (to render it opaque) and an aperture formed at its apex. Figure 9a shows a scanning electron microscopy (SEM) image of a typical pyramidal probe. Figure 9b shows a high magnification image of the apex of the probe, revealing the aperture. The width of the aperture was found to be ca. 150 nm. The probe was operated in contact with the sample surface.

Figure 9c shows a friction image of a series of lines fabricated on a SAM adsorbed on an aluminum oxide surface using the near-field probe. The samples were exposed in air, causing degradation of the azide. As described above, the product of the degradation process could be amines, formed by reduction of the photochemically generated nitrene, diazo compounds, or more complex polymers (formed by the reactions of nitrenes with neighboring azides, or through ketenamine reactions with themselves in the absence of good nucleophiles).[43] The product has a slightly higher surface free energy than the unmodified azide, and so it exhibits brighter contrast in the FFM image. Analysis of a line section through a higher magnification image (Figure 9d) showed that the line width was 150 nm, similar to the size of the aperture in the near-field probe, confirming that resolution is limited by the aperture dimensions.

After creating features by near-field lithography, the unreacted surrounding surface could be modified in a second maskless step. Figure 9 (panels e and f) show two identical patterns that have been formed in such a two-stage process. The first step is the ambient exposure of the aryl azide terminated SAM to the near-field probe. This causes localized degradation of the azide. The remaining unmodified azides may then be used to couple a primary amine to the surface in a second step, by exposing the whole sample to UV light while immersed under a film of the amine. Figure 9e shows a friction image of a sample where the second step has been carried out under a film of octadecylamine. The methyl-terminated amine has a low surface free energy and thus exhibits darker contrast than the surface formed by near-field modification of the azide. If, instead, the second step is carried out with the sample immersed under a film of ethanolamine, then a contrast

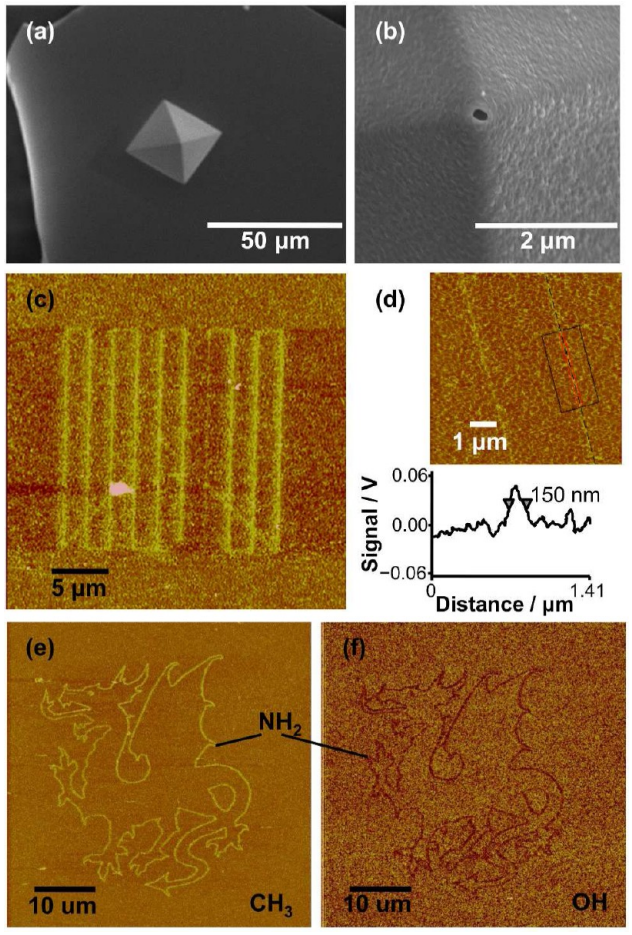

Figure 9. (a and b) Scanning electron micrographs of a typical near-field probe at different magnifications. (c and d) FFM images of features formed by exposure of aryl azide terminated SAMs on aluminum oxide under ambient conditions. (e and f) FFM images of two identical patterns formed by initial ambient near-field exposure of aryl azide terminated SAMs followed by subsequent, maskless exposure under films of (e) octadecylamine and (f) ethanolamine.

inversion is observed in the resulting FFM image, with the hydroxyl functionalized regions exhibiting brighter contrast (i.e., higher friction because of a higher surface free energy) than the pattern written by the near-field probe. While in these examples the initial exposure was carried out under ambient conditions, near-field lithography has been shown to be feasible under fluid,[61] so with suitable adaptation of the apparatus, both steps could be carried out with the sample immersed under a reagent.

Figure 10 demonstrates the feasibility of patterning proteins using a simple adaptation of this approach. A schematic diagram shows the methodology: initial exposure of the surface may be carried out using either a mask or a near-field probe, to degrade the azide groups and define protein-adhesive regions; the remainder of the sample is subsequently functionalized with a protein-resistant oligo(ethylene glycol)-terminated primary amine, rendering them nonadhesive. Simple immersion of the sample into a solution of the protein in buffer will yield a protein pattern through nonspecific adsorption of protein onto the regions patterned in the first step. Figure 10(a−c) show fluorescence images of patterns formed using either a mask-based or a near-field exposure. In place of a protein, NeutrAvidin-coated dye-labeled polymer nanoparticles have

dx.doi.org/10.1021/la303746e | Langmuir 2013, 29, 1083−1092

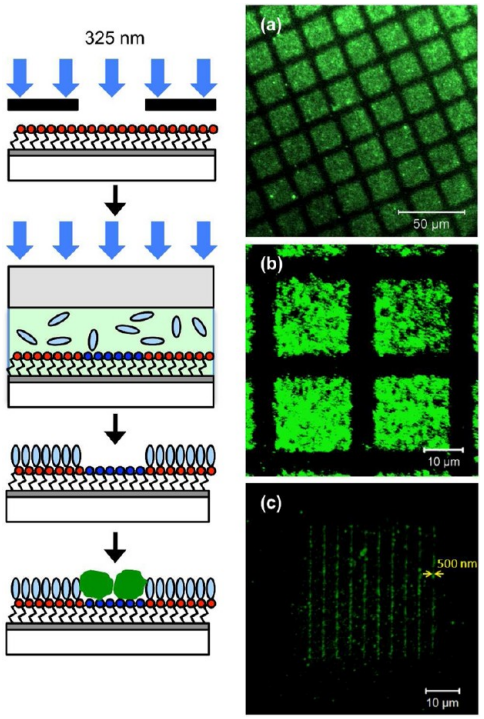

Figure 10. Schematic showing selective deactivation of azides by photopatterning, followed by passivation of remaining regions by attachment of oligo(ethylene glycol)-terminated amines and adsorption of NeutrAvidin-functionalized nanoparticles into patterned regions (left). Confocal fluorescence microscopy images of samples prepared by micropatterning with (a and b) a mask and (c) near-field exposure in the first step (right).

been used; these replicate the adhesive properties of proteins while yielding good contrast in fluorescence microscopy. It can be seen that fluorescence is weak from the oligo(ethylene glycol)-functionalized regions of the surface, indicating a good resistance to nonspecific adsorption, but strong from the regions exposed to UV radiation using either mask-based or near-field photolithography, indicating both effective deactivation of the azide and adhesion of the nanoparticles. Although the interaction between the NeutrAvidin-coated particles and the surface is not a specific one here, the process could be adapted to facilitate specific attachment, for example, through the attachment of nitrilotriacetic acid or biotin to the amine-functionalized regions and subsequent binding of, respectively, a histidine-tagged protein or avidin.

CONCLUSIONS

Aryl azide terminated monolayers are degraded by exposure to near UV radiation and react with primary amines when exposed to UV radiation under a film of the amine. The extent of derivatization is greater for aryl azide terminated SAMs than for diazirine-functionalized monolayers. The fraction of the terminal azides that reacts with the primary amine is high, and a wide variety of amines has been found to react. No advantages were found when using the more complex diazirine, nor the fluoroazide. The coupling chemistry is thought to be based on either insertion into NH bonds, or nucleophilic addition to the ring-expanded ketenamine. The reaction must occur in situ, as photo reaction in air creates surfaces that no longer react with primary amines. If this analysis is correct, then site-selective trapping of solution-phase substrates may be feasible; studies are ongoing concerning this question. By using a photolithographic exposure process to spatially define the reactivity of the aryl azide with the primary amine, it is possible to fabricate micrometer or nanometer scale patterns, by using mask-based and near-field processes, respectively. Protein patterns can be produced by defining adhesive regions in the lithographic step and passivating the remaining surface with an oligo(ethylene glycol)-functionalized amine. The wide variety of amines that are available commercially and the simplicity of the photochemical-coupling chemistry suggest that such approaches should be of widespread utility in surface chemistry and in micro- and nanofabrication and may offer some promise in the attempt to integrate top-down (lithographic) approaches with bottom-up (synthetic chemical) ones.

ASSOCIATED CONTENT

Supporting Information

Full details of the synthesis of the molecules used in this study and detailed quantitative data following 4-chlorobenzylamine photocoupling reactions. This material is available free of charge via the Internet at http://pubs.acs.org.

AUTHOR INFORMATION

Corresponding Author

*N.H.W.: e-mail, N.H.Williams@sheffield.ac.uk. G.J.L.: e-mail, Graham.Leggett@sheffield.ac.uk.

Present Address

[†]Department of Chemistry, Faculty of Science, University of Malaya, 50603 Kuala Lumpur, Malaysia.

Funding

The authors thank EPSRC (Grant EP/050271/1) and RCUK (Grant EP/C523857/1) for financial support.

Notes

The authors declare no competing financial interest.

REFERENCES

(1) Ginger, D. S.; Zhang, H.; Mirkin, C. A. *Angew. Chem., Int. Ed.* **2004**, *43*, 30.
(2) Hong, S.; Zhu, J.; Mirkin, C. A. *Science* **1999**, *286*, 523.
(3) Piner, R. D.; Zhu, J.; Xu, F.; Hong, S.; Mirkin, C. A. *Science* **1999**, *283*, 661.
(4) Liu, G.-Y.; Amro, N. A. *Proc. Natl. Acad. Sci. U.S.A.* **2002**, *99*, 5165.
(5) Amro, N. A.; Xu, S.; Liu, G.-Y. *Langmuir* **2000**, *16*, 3006.
(6) Maoz, R.; Cohen, S. R.; Sagiv, J. *Adv. Mater.* **1999**, *11*, 55.
(7) Maoz, R.; Frydman, E.; Cohen, S. R.; Sagiv, J. *Adv. Mater.* **2000**, *12*, 424.
(8) Fresco, Z. M.; Frechet, J. M. J. *J. Am. Chem. Soc.* **2005**, *127*, 8302.
(9) Sun, S.; Chong, K. S. L.; Leggett, G. J. *J. Am. Chem. Soc.* **2002**, *124*, 2414.
(10) Sun, S.; Leggett, G. J. *Nano Lett.* **2004**, *4*, 1381.
(11) Montague, M.; Ducker, R. E.; Chong, K. S. L.; Manning, R. J.; Rutten, F. J. M.; Davies, M. C.; Leggett, G. J. *Langmuir* **2007**, *23*, 7328.
(12) Leggett, G. J. *Nanoscale* **2012**, *4*, 1840.
(13) Alang Ahmad, S. A.; Wong, L. S.; ul-Haq, E.; Hobbs, J. K.; Leggett, G. J.; Micklefield, J. *J. Am. Chem. Soc.* **2011**, *133*, 2749.
(14) Fodor, S. P.; Read, J. L.; Pirrung, M. C.; Stryer, L.; Lu, A. T.; Solas, D. *Science* **1991**, *251*, 767.
(15) Pirrung, M. C.; Huang, C.-Y. *Bioconjugate Chem.* **1996**, *7*, 317.
(16) Pirrung, M. C.; Wang, L.; Montague-Smith, M. P. *Org. Lett.* **2001**, *3*, 1105.
(17) Critchley, K.; Ducker, R.; Bramble, J. P.; Zhang, L.; Bushby, R. J.; Leggett, G. J.; Evans, S. D. *J. Exp. Nanosci.* **2007**, *2*, 278.
(18) Alang-Ahmad, S. A.; Wong, L. S.; ul-Haq, E.; Hobbs, J. K.; Leggett, G. J.; Micklefield, J. *J. Am. Chem. Soc.* **2009**, *131*, 1513.

(19) Critchley, K.; Jeyadevan, J. P.; Fukushima, H.; Ishida, M.; Shimoda, T.; Bushby, R. J.; Evans, S. D. *Langmuir* **2005**, *21*, 4554.
(20) Wöll, D.; Laimgruber, S.; Galetskaya, M.; Smirnova, J.; Pfleiderer, W.; Heinz, B.; Gilch, P.; Steiner, U. E. *J. Am. Chem. Soc.* **2007**, *129*, 12148.
(21) Critchley, K.; Zhang, L.; Fukushima, H.; Ishida, M.; Shimoda, T.; Bushby, R. J.; Evans, S. D. *J. Phys. Chem. B* **2006**, *110*, 17167.
(22) Yang, Z.; Frey, W.; Oliver, T.; Chilkoti, A. *Langmuir* **2000**, *16*, 1751.
(23) Nakayama, K.; Tachikawa, T.; Majima, T. *Langmuir* **2008**, *24*, 6425.
(24) Petersen, S.; Alonso, J. M.; Specht, A.; Duodo, P.; Goeldner, M.; Campo, A. d. *Angew. Chem., Int. Ed.* **2008**, *47*, 3192.
(25) Bhagawati, M.; Lata, S.; Tampee, R.; Piehler, J. *J. Am. Chem. Soc.* **2010**, *132*, 5932.
(26) Weinrich, D.; Köhn, M.; Jonkheijm, P.; Westerlind, U.; Dehmelt, L.; Engelkamp, H.; Christianen, P. C. M.; Kuhlmann, J.; Maan, J. C.; Nüsse, D.; Schröder, H.; Wacker, R.; Voges, E.; Breinbauer, R.; Kunz, H.; Niemeyer, C. M.; Waldmann, H. *ChemBioChem* **2010**, *11*, 235.
(27) Orski, S. V.; Poloukhtine, A. A.; Arumugam, S.; Mao, L.; Popik, V. V.; Locklin, J. *J. Am. Chem. Soc.* **2010**, *132*, 11024.
(28) Huisgen, R. *Proc. Chem. Soc., London* **1961**, 357.
(29) Kolb, H. C.; Finn, M. G.; Sharpless, K. B. *Angew. Chem., Int. Ed.* **2001**, *40*, 2004.
(30) Yan, M.; Ren, J. *Chem. Mater.* **2004**, *16*, 1627.
(31) Burdzinski, G.; Hackett, J. C.; Wang, J.; Gustafson, T. L.; Hadad, C. M.; Platz, M. S. *J. Am. Chem. Soc.* **2006**, *128*, 13402.
(32) Wilson, C. G. In *Introduction to Microlithography*; Thompson, L. F., Ed.; ACS: 1994, p 160.
(33) Wollman, E. W.; Kang, D.; Frisbie, C. D.; Lorkovic, I. M.; Wrighton, M. S. *J. Am. Chem. Soc.* **1994**, *116*, 4395.
(34) Keana, J. F. W.; Cai, S. X. *J. Org. Chem.* **1990**, *55*, 3640.
(35) Soundararajan, N.; Platz, M. S. *J. Org. Chem.* **1990**, *55*, 2034.
(36) Leyva, E.; Platz, M. S.; Persy, G.; Wirz, J. *J. Am. Chem. Soc.* **1986**, *108*, 3783.
(37) Leyva, E.; Platz, M. S. *Tetrahedron Lett.* **1985**, *26*, 2147.
(38) Marcinek, A.; Leyva, E.; Whitt, D.; Platz, M. S. *J. Am. Chem. Soc.* **1993**, *115*, 8609.
(39) Leyva, E.; Young, M. J. T.; Platz, M. S. *J. Am. Chem. Soc.* **1986**, *108*, 8307.
(40) Leyva, E.; de Loera, D.; Leyva, S. *Tetrahedron Lett.* **2008**, *49*, 6759.
(41) McClelland, R. A.; Davidse, P. A.; Hadzialic, G. *J. Am. Chem. Soc.* **1995**, *117*, 4173.
(42) Novak, M.; Rajagopal, S. In *Advances in Physical Organic Chemistry*; Academic Press: London, 2001; Vol. *36*, p 167.
(43) Cline, M. R.; Mandel, S. M.; Platz, M. S. *Biochemistry* **2007**, *46*, 1981.
(44) Gritsan, N. P.; Tigelaar, D.; Platz, M. S. *J. Phys. Chem. A* **1999**, *103*, 4465.
(45) Pritchard, D. J.; Morgan, H.; Cooper, J. M. *Anal. Chem.* **1995**, *67*, 3605.
(46) Blawas, A. S.; Reichert, W. M. *Biomaterials* **1998**, *19*, 595.
(47) Al-Bataineh, S. A.; Luginbuehl, R.; Textor, M.; Yan, M. *Langmuir* **2009**, *25*, 7432.
(48) Wang, X.; Ramstrom, O.; Yan, M. *J. Mater. Chem.* **2009**, *19*, 8944.
(49) Liu, L.-H.; Yan, M. *Acc. Chem. Res.* **2010**, *43*, 1434.
(50) Liu, L.-H.; Zorn, G.; Castner, D. G.; Solanki, R.; Lerner, M. M.; Yan, M. *J. Mater. Chem.* **2010**, *20*, 5041.
(51) Fairley, N. *CasaXPS*; Casa Software Ltd.: Teignmouth, U.K., 2009; (http://www.casaxps.com).
(52) Lamara, K.; Smalley, R. K. *Tetrahedron* **1991**, *47*, 2277.
(53) Leyva, E.; Platz, M. S.; Persy, G.; Wirz, J. *J. Am. Chem. Soc.* **1986**, *108*, 3783.
(54) Liang, T.-Y.; Schuster, G. B. *J. Am. Chem. Soc.* **1987**, *109*, 7803.
(55) Frisbie, C. D.; Wollman, E. W.; Wrighton, M. S. *Langmuir* **1995**, *11*, 2563.
(56) Dubey, M.; Weidner, T.; Gamble, L. J.; Castner, D. G. *Langmuir* **2010**, *26*, 14747.
(57) Overney, R.; Meyer, E. *MRS Bull.* **1993**, *26*.
(58) Grafstrom, S.; Neitzert, M.; Hagen, T.; Ackerman, J.; Neumann, R.; Probst, O.; Wortge, M. *Nanotechnol.* **1993**, *3*, 143.
(59) Carpick, R. W.; Salmeron, M. *Chem. Rev.* **1997**, *97*, 1163.
(60) Busuttil, K.; Geoghegan, M.; Hunter, C. A.; Leggett, G. J. *J. Am. Chem. Soc.* **2011**, *133*, 8625.
(61) Haq, E. u.; Liu, Z.; Zhang, Y.; Ahmad, S. A. A.; Wong, L.-S.; Armes, S. P.; Hobbs, J. K.; Leggett, G. J.; Micklefield, J.; Roberts, C. J.; Weaver, J. M. R. *Nano Lett.* **2010**, *10*, 4375.